International Journal of Rock Mechanics & Mining Sciences 47 (2010) 405–413

Contents lists available at ScienceDirect

International Journal of Rock Mechanics & Mining Sciences

journal homepage: www.elsevier.com/locate/ijrmms

A numerical model for fluid injection induced seismicity at Soultz-sous-Forêts

Stefan Baisch [a], Robert Vörös [a], Elmar Rothert [a,*], Henrik Stang [a], Reinhard Jung [b,1], Rüdiger Schellschmidt [c]

[a] Q-con GmbH, Marktstr. 39, 76887 Bad Bergzabern, Germany
[b] Jung-Geotherm, Gottfried-Buhr-Weg 19, 30916 Isernhagen, Germany
[c] Leibniz Institute for Applied Geophysics, Stilleweg 2, 30655 Hannover, Germany

ARTICLE INFO

Article history:
Received 28 May 2009
Received in revised form
14 August 2009
Accepted 4 October 2009
Available online 7 November 2009

Keywords:
Reservoir induced seismicity
Numerical simulations
Earthquake mechanics
Geothermal
Seismic risk

ABSTRACT

During fluid injection experiments at the geothermal site of Soultz-sous-Forêts (France), more than 114,000 induced seismic events with magnitudes between −2.0 and +2.9 were detected by a local downhole monitoring network. Of these, 35,039 events are sufficiently constrained to be located. Hypocenters align along a sub-vertical, planar structure with the apparent width being dominated by data scattering indicating that seismic activity predominantly occurs along a (pre-existing) larger scale fault structure. For this scenario, we present a numerical model to simulate hydraulic overpressures and induced seismicity during hydraulic injection. The numerical model is based on the physical processes of fluid pressure and stress diffusion with triggering of the induced seismicity being controlled by Coulomb friction.

Even in its simplest form of a fault zone without any structural heterogeneity, the numerical model reproduces typical observations at Soultz-sous-Forêts, such as number and magnitude of induced events, hypocenter locations (including the Kaiser effect), occurrence of post-injection seismicity, and the largest magnitude event occurring several days after shut-in.

1. Introduction

Shear dilation stimulation, which implies injection of large fluid volumes at high pressure, has become a standard technology for the development of deep geothermal reservoirs (enhanced geothermal systems, EGS). Especially in crystalline host rock, these stimulations are accompanied by vast amounts of induced seismicity [1,2]. Although most of the induced seismicity is of small magnitude below the human detection threshold, isolated events of larger magnitude were induced in the past (Table 1).

The most prominent example is an M=3.4 event induced by the stimulation of a geothermal reservoir below the city of Basel (Switzerland) which led to a (preliminary) termination of the project [3]. At the geothermal site of Soultz-sous-Forêts (France), stimulation of the deep reservoir produced seismic events with magnitudes of up to M=2.9 [4] raising major concerns about potential damage. After the largest magnitude event (M=2.9) occurred in 2003, the stimulation strategy had been modified by using lower flow rates and smaller volumes of injection fluid at Soultz-sous-Forêts. However, the physical mechanisms leading to large magnitude events are not well understood yet. Interestingly, the largest magnitude events seem to occur predominantly in the shut-in period after fluid injection has been terminated (Table 1). This complicates the application of "traffic light systems" where hydraulic injection is aborted whenever seismicity exceeds a critical magnitude threshold [5]. Clearly, a more detailed understanding of the physical processes associated with induced seismicity is required to enable a large scale application of the EGS technology [1].

We have developed a numerical model to simulate induced seismicity during hydraulic stimulations. Based on the observed hypocenter distribution at Soultz-sous-Forêts, induced seismicity is assumed to occur on a single (subvertical), large scale fracture zone. Following previous considerations, the fracture zone is assumed to be of tectonic origin [6] and may have formed as part of the Rhine–Graben structure [4]. In this model, the pre-existing fracture zone provides the dominating fluid pathway during hydraulic stimulation and the induced seismicity is controlled by Coulomb friction.

We numerically simulate hydraulic overpressures in a two-dimensional fracture zone with the finite element method by solving the diffusion equation (see, e.g. [7]). The fracture zone consists of individual blocks of 20 metres side length which can slip independently but are mechanically coupled to their neighbouring patches ("block-spring model", e.g. [8]). Once

* Corresponding author. Tel.: +49 6343939699; fax: +49 6343939729.
E-mail addresses: baisch@q-con.de (S. Baisch), rothert@q-con.de (E. Rothert).
[1] Former Leibniz Institute for Applied Geophysics, now at Jung-Geotherm.

1365-1609/$ - see front matter © 2009 Elsevier Ltd. All rights reserved.
doi:10.1016/j.ijrmms.2009.10.001

fracture criticality of an individual block is exceeded, slippage occurs and results in a constant (shear-) stress drop of this particular block. Dynamic stress transfer to neighbouring blocks may result in slip avalanches. Due to the *a priori* assumption of a constant stress drop, event magnitudes are solely determined by the slip area, i.e. the number of block patches slipping simultaneously. Following the concept of self-propping (e.g. [9]) hydraulic permeability of patches increases by slipping.

Our model parameters are chosen to be consistent with parameters observed at Soultz-sous-Forêts, although we kept the numerical model as simple as possible. Despite its simplicity, modelling results sufficiently match first order observations at Soultz-sous-Forêts, such as hydraulic overpressures, the spatio-temporal distribution of induced seismicity, event rates, event magnitudes, and the occurrence of large magnitude, post-injection seismicity.

Table 1
Maximum earthquake magnitude of events associated with hydraulic stimulation in selected EGS projects.

EGS project	Activity	M_{max}	Refs.
Soultz-sous-Forêts (France)	Stimulation well GPK4	2.3*	[25]
Soultz-sous-Forêts (France)	Stimulation well GPK2	2.4*	[28]
Cooper Basin (Australia)	Re-stimulation well H#1	2.9	[27]
Soultz-sous-Forêts (France)	Stimulation well GPK3	2.9*	[4]
Basel (Switzerland)	Stimulation well Basel1	3.4*	[3]
Cooper Basin (Australia)	Stimulation well H#1	3.7*	[11]
Berlín Field (El Salvador)	Stimulation well TR8A	4.4*	[5]

Asterisks denote events occurring post stimulation during shut-in of the injection well.

2. Induced seismicity at Soultz-sous-Forêts

The Soultz-sous-Forêts (France) geothermal site is situated within the central part of the Upper Rhine Graben approximately 50 km north of Strasbourg. The local geology is characterized by highly fractured granite overlain by approximately 1400 m sedimentary coverage. Geothermal research activities at Soultz-sous-Forêts started in 1987. Besides several shallower wells, today there exist three approximately 5000 m deep wells [4]. Several massive

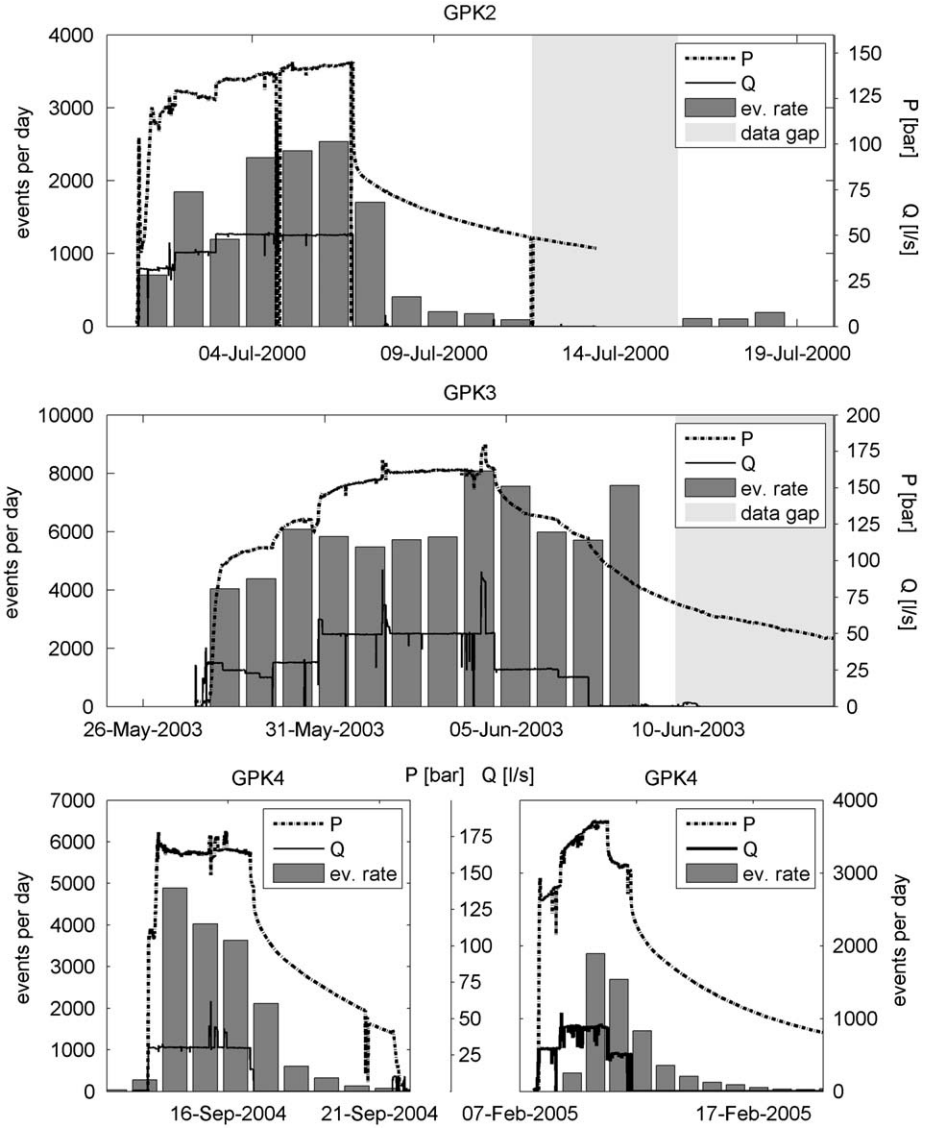

Fig. 1. Hydraulic wellhead pressure (dotted line), injection rates (solid line), and rate of induced events (bars) as a function of time for the stimulation of well GPK2 (top), GPK3 (middle), and GPK4 (bottom). The well GPK4 has been stimulated twice, in 2004 (bottom, left), and in 2005 (bottom, right). Grey shading denotes data gaps for which no seismic recordings were available.

hydraulic stimulations have been performed to create a subsurface heat exchanger below 4000 m depth. In the year 2000, the well GPK-2 has been stimulated by injecting approximately 23,000 m^3 of water at flow rates of 30–50 l/s and overpressures of up to 13 MPa (Fig. 1, top). A second well, GPK-3, has been stimulated in the year 2003 by injecting approximately 37,000 m^3 of water at similar flow rates and overpressures (Fig. 1, middle). The third well, GPK4, has been stimulated twice (Fig. 1, bottom) by injecting a total volume of approximately 22,000 m^3.

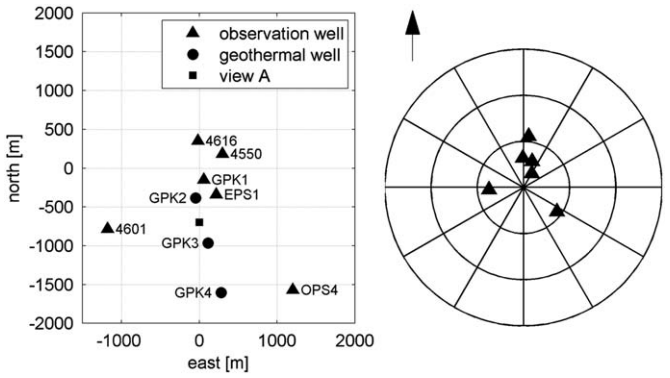

Fig. 2. Left: Seismic stations (triangles) and location of geothermal wells (circles) in map view. Right: Upper hemisphere stereographic projection of the station locations viewed from 4400 m depth at the location labelled "view A" in left hand panel. Instrument deployment depths are between 1500 and 3500 m. Note that station 4616 was deployed only during the stimulations of GPK4.

Hydraulic stimulation activities were monitored with a local seismic network consisting of multi-component downhole instruments (accelerometers and geophones) deployed in observation boreholes between 1500 and 3500 m depth (Fig. 2, left).

More than 114,000 seismic events were detected during the stimulation of the three wells with rates up to 8000 events per day (Fig. 1, middle). Among these, however, a considerable number of events were of low magnitude and thus recorded by the deepest instrument (deployed in GPK1 at 3500 m depth) only.

To merely consider sufficiently constrained hypocenter locations, we selected those events for which at least eight phase onsets could be determined. Due to the extreme sparsity of the station network, large azimuthal gaps or even a coplanar network configuration may result if a single instrument provides no data. This is illustrated in Fig. 2 (right) which shows the station distribution viewed from a location inside the reservoir. Azimuthal coverage is critically dependent on stations 4601 and OPS4 and

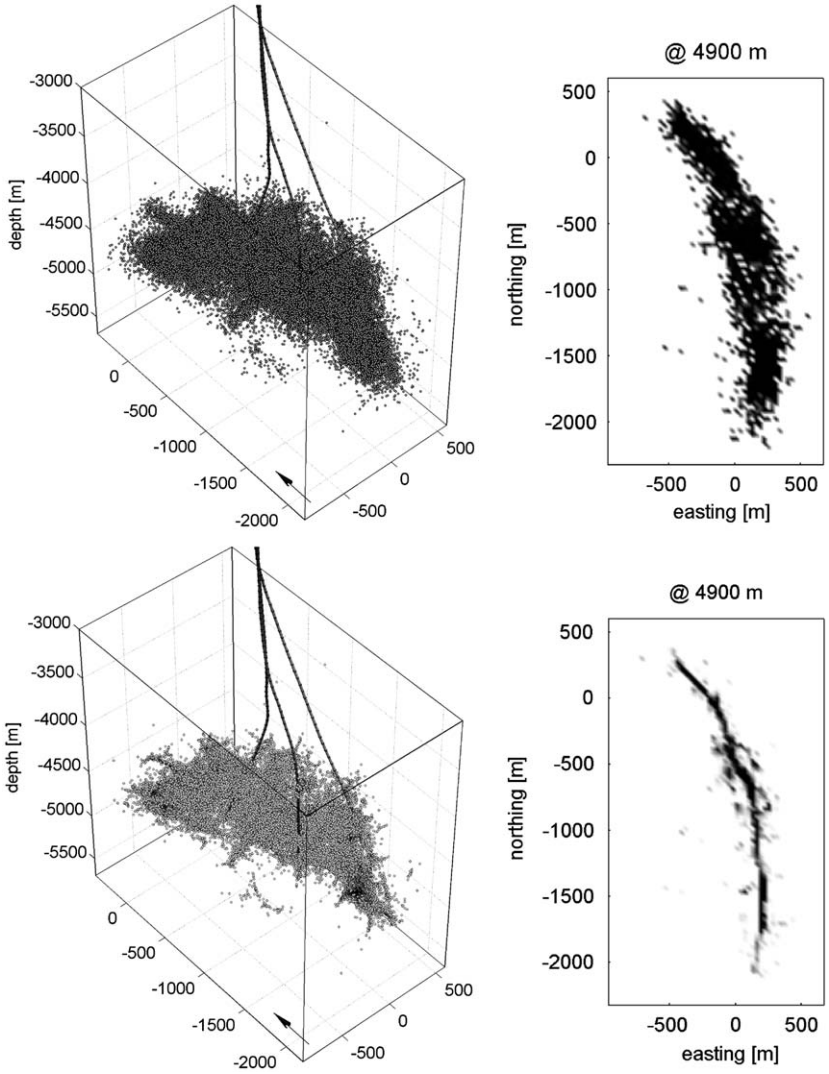

Fig. 3. Top left: Hypocenter distribution in perspective view. Solid lines indicate the trajectories of GPK2, GPK3, and GPK4, respectively. Top right: Depth slice of the hypocenter density distribution at 4900 m depth. Dark shading denotes regions of high density. Bottom: same as above after applying data collapsing.

therefore we additionally require that at least three phase onsets can be determined at these stations.

Our hypocenter location procedure follows the approach of Baisch et al. [10], where absolute hypocenter locations and station residuals are determined iteratively based on a linearized inversion. A homogeneous seismic velocity model has been calibrated by associating early seismicity during the GPK3 stimulation to the dominating flow exit at 4760 m logging depth (for details about this approach we refer to [11]). With the resulting velocities of V_p=5585 m/s and V_s=3295 m/s, station residuals are 8 ms or less indicating that the underlying velocity model is consistent with the current data set. Fig. 3 (top, left) shows the hypocenter distribution for those 35,039 events which meet the selection criteria. Average location errors on a 2σ confidence level are 67, 68, and 59 m in the eastern, northern, and vertical directions, respectively.

The hypocenter distribution is dominated by a subvertical, north–south trending structure of approximately 2500 m lateral, and 1000 m vertical extension. Towards the north, the main structure slightly rotates into the north–west. The apparent east–west thickness of the structure is in the order of 300–500 m (Fig. 3, top right). Considering location errors, however, it can be assumed that the true thickness of the structure will be much smaller. We have experimented with different relative hypocenter location techniques to reduce the effect of data scattering. Due to the varying data quality and repeated modifications of (analogue) filter settings, automatic data processing was complicated. Relative hypocenter locations could be determined (automatically) only for a smaller fraction of the entire data set and are therefore not shown.

A technique frequently used for enhancing structures in hypocenter clouds is the collapsing method of Jones and Stewart [12]. Fig. 3 (bottom, left) shows the hypocenter distribution after applying the collapsing method on a 4σ confidence level. Most hypocenters align along a single, planar structure and the east–west thickness of the structure is substantially reduced, frequently down to the resolution limit (Fig. 3, bottom right). Although collapsed data need to be interpreted with care, our results nevertheless indicate that the observed seismicity distribution at Soultz-sous-Forêts can be consistently aligned (within confidence limits) along a single, subvertical planar structure.

3. Hydro-mechanical reservoir model

In the previous section we found evidence that the seismically active region is dominated by a subvertical, planar structure. This structure was previously interpreted as a large scale fault zone, potentially being part of the Rhine-Graben system [13]. The existence of such a structure is also supported by the fact that relatively large magnitude events have occurred in the reservoir which typically require shearing planes in the order of several tens of thousands metres squared. Although the seismicity distribution (Fig. 3) exhibits a small degree of curvature and potentially some complexity on a local scale, we nevertheless approximate the reservoir geometry by the simplest geometrical model of a single, subvertical plane. Thereby we limit our study to first order effects. We note, however, that more complicated models with spatially varying fault properties cannot be calibrated by the current data.

Borehole imaging data obtained from the GPK3 well resolve a major damage zone at 4760 m depth where the near-well seismicity is concentrated. During stimulation of GPK3, most of the fluid left the injection well through this particular damage zone. Consistent with our geometrical reservoir model, these observations indicate that the seismically active structure also coincides with the dominating fluid pathway. From logging information it is not clear whether or not the damage zone observed in GPK3 is of natural origin (i.e. existed before the stimulations) or has been formed during hydraulic operations. The hydraulic response of the reservoir during stimulation (Fig. 1, middle) may argue against a model where the damage zone has been formed by a jacking tensile fracture. In this case a well defined limitation of the hydraulic overpressures could be expected which was not observed. Furthermore, stress estimates by different authors (summarized in [14]) indicate that the least principal stress has not been exceeded by in situ fluid pressures during the stimulation of GPK3. This further supports a model where the reservoir is dominated by a pre-existing, tectonically formed structure.

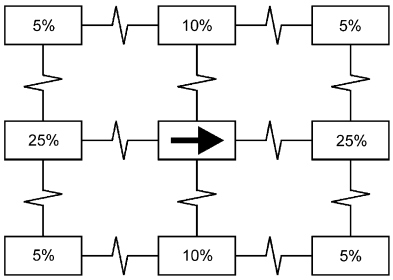

Fig. 4. Sketch of stress redistribution for slip on the central patch. Amount of shear–stress redistribution is indicated in percent of the stress drop on the central patch.

Below the jacking pressure, the mechanisms causing induced seismicity can be explained by hydraulic overpressures reducing the effective normal stress on existing fractures [15]. Let τ and σ_n denote the shear and normal stresses resolved on a fracture plane, P_{fl} the in situ fluid pressure, and μ the coefficient of friction, then slip occurs on the fracture if

$$\tau/(\sigma_n - P_{fl}) > \mu \tag{1}$$

We assume that the large-scale fault consists of many smaller fault patches which may slip independently but are mechanically coupled to their neighbours (so called "block-spring model", e.g. [8]). Slip occurs whenever the resolved shear stress on a patch exceeds the frictional strength. Thereby the shear stress resolved on the patch is reduced by the amount of stress drop $\Delta\tau$ and shear stress on the neighbouring patches is increased due to mechanical coupling. Fig. 4 sketches the stress transfer pattern implemented in our model. Consistent with previous studies (e.g. [16]), an overall stress transfer of 90% is assumed.

Due to stress redistribution, slip on an individual patch may cause overcritical stress conditions on neighbouring patches, thus triggering an "avalanche" of simultaneous slip events. The strength of a seismic shear event can be described by its seismic moment M_0 which is determined by

$$M_0 = GAd \tag{2}$$

with shear modulus G, fracture plane area A, and slip displacement d. Assuming that variations of d are small compared to variations of A, then the strength of an earthquake is primarily determined by the number of patches slipping simultaneously.

4. Numerical simulations

We implemented the conceptual model discussed in the previous section into a numerical finite-element model. The numerical model consists of a subvertical, rectangular structure, representing a fault zone, which is intersected by a well at a depth of 4800 m. The fault zone extends over 3 km in both lateral and

vertical direction. To avoid boundary effects, the model is augmented at the outer rim of the fault zone to a total extension of 20 km × 20 km with constant pressure boundaries. For simplicity we assume a constant 48 MPa hydrostatic pressure in the fault zone corresponding to the nominal hydrostatic fluid pressure at the intersection depth with the well.

Although we did not attempt to exactly model the Soultz-sous-Forêts stimulation operations, our model parameters are chosen such that they are approximately consistent with parameters observed at Soultz-sous-Forêts. The stress field is adopted from Cornet et al. [14] with maximum and minimum stresses being horizontally oriented and S_H striking at N170°. Resulting shear and normal stresses acting on the fault zone are 27 and 79 MPa, respectively. A coefficient of friction of μ=0.9 is assumed which is slightly larger than μ=0.88 estimated by Cornet et al. [14]. We note, however, that a larger value for the coefficient of friction is required to obtain stable stress conditions in our model prior to the injection.

Table 2
Parameters of the numerical model.

Parameter	Symbol	Value	Units
Initial transmissibility	T	10	mDm
Storage coefficient	S	5e−9	m/Pa
Dyn. viscosity	μ	2.4e−4	Pa s
Width	h	1	mm
Well radius	rw	0.1	m
Stress drop	$\Delta\tau$	1	MPa
Sampling interval	Δt	1	s

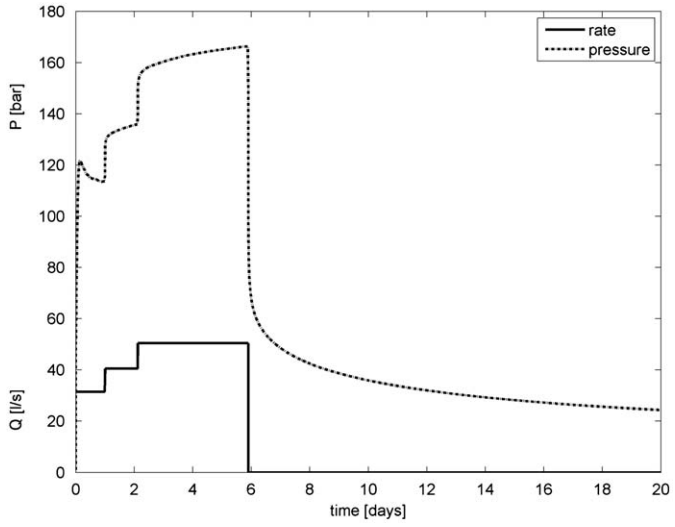

Fig. 5. Injection rate (solid line) and modelled wellhead pressure (dotted line). Injection rates approximate the GPK2 injection history (compare Fig. 1, top).

The fault is divided into quadratic patches of 20 m side length. We assume that slipping of a patch (whenever the ratio between shear to effective normal stress exceeds the frictional strength of the patch; see Eq. (1)) causes an increase of the permeability for the associated patch, thus leading to spatio-temporal changes of the permeability in the model. At each time step, the parameter distribution is updated according to our mechanical model and the fluid pressure for the next time sample is computed by solving the diffusion equation with respect to the updated distribution. We assume a local permeability enhancement of 10% for each slip and limit the maximum possible enhancement to be 100-fold. The storage coefficient remains unaffected by the stimulation. Hydraulic parameters assumed in the numerical model (summarized in Table 2) are within the range of parameters determined previously by Tischner et al. [17]. In contrast to their study, our conceptual model consists of a small aperture fracture instead of the wider fault zone assumed in [17]. Since we assume a similar permeability–thickness product (transmissibility), the hydraulic responses of our model and that of [17] are comparable. However, unlike to the model described in [17], we assume a large storage coefficient to compensate for unmodelled, small-scale elastic storage effects.

Fig. 5 shows simulated overpressures ("wellhead" pressure) for an injection history similar to the GPK2 stimulation. Simulated overpressures are of the same order of magnitude as the observed hydraulic response during the GPK2 stimulation, although there exist significant differences which will be discussed in a later section. A total of 24,872 slip events were triggered during the 20 day simulation period. The seismic moment (Eq. (2)) of these events varies between 10^9 and 10^{13} Nm. This corresponds to a magnitude range of $M=-1.1$ to $M=+2.8$ when using the empirical formula of Bungum et al. [18]. Fig. 6 shows the temporal evolution of the modelled event magnitudes. Besides a few scattered events with comparatively large magnitudes (i.e. around M=2) occurring at an early stage of the injection, the maximum event magnitude tends to increase with time during the stimulation. This becomes most evident during shut-in and we notice that the largest magnitude event occurred approximately 6.5 days after shut-in. As will be discussed later, the increase of the maximum event magnitude can be attributed to a simple geometrical effect where

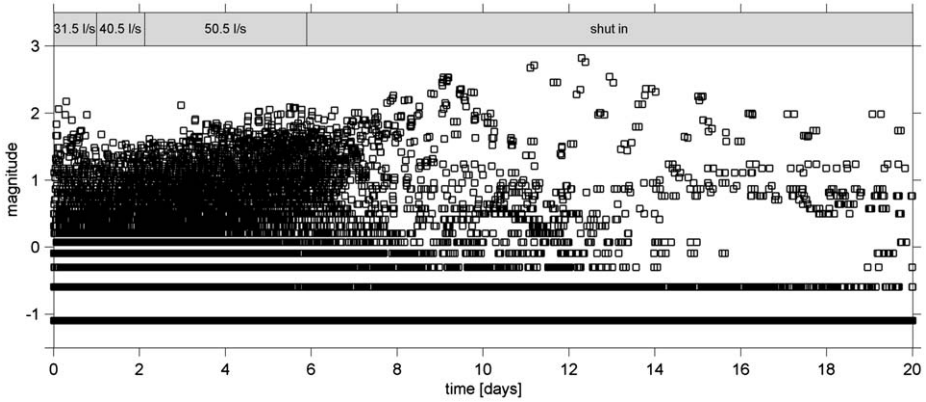

Fig. 6. Magnitude of the modelled seismicity as a function of time. Top bar indicates the injection history. Note that the largest magnitude events occurred post-injection. The discrete magnitude distribution (most prominent at the lower magnitude end) results from the assumptions of constant stress drop in combination with a discrete patch size.

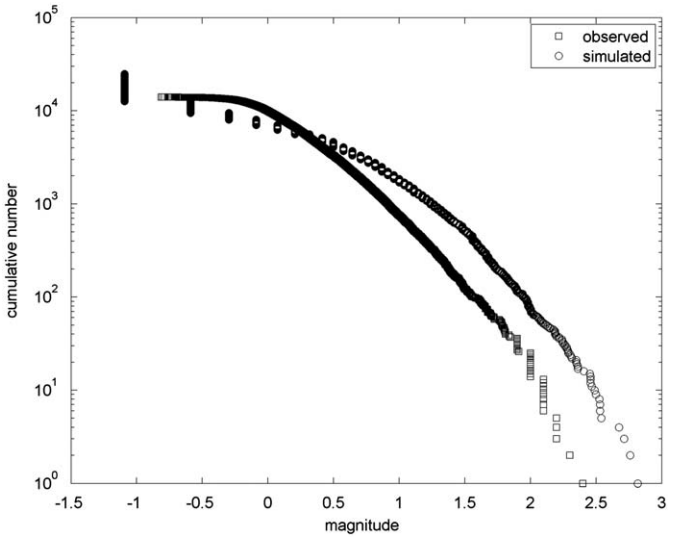

Fig. 7. Magnitude frequency distribution of seismic events observed during the stimulation of GPK2 (squares) and modelled seismicity (circles).

the area over which fluid overpressure is acting growths with time.

Modelled and observed seismicity exhibit similar characteristics with respect to the total number of events and the event magnitude distribution, respectively. This becomes most evident in Fig. 7, which compares the two magnitude–frequency distributions. The slope of the two distributions is similar, although modelled magnitudes systematically exceed observed values by approximately 0.4 magnitude units. We note, however, that the two magnitude scales might not be strictly comparable due to different magnitude definitions and the empirical relationship used to convert seismic moment into moment magnitude which is strictly valid only for magnitudes M_L between 0 and 2.

5. Discussion

We have presented a numerical model to simulate hydraulic overpressures and induced seismicity for an injection experiment conducted at the geothermal site at Soultz-sous-Forêts. The model is based on the physical processes of fluid pressure and stress diffusion with triggering of the induced seismicity being controlled by Coulomb friction. Although model parameters are chosen to be consistent with parameters observed at Soultz-sous-Forêts, the numerical model is kept as simple as possible whenever parameters could not be constrained by observations. Initially, our structural model has no spatial complexity, consisting of a single (effectively infinite) fracture with no variations of resolved stresses or hydraulic properties, respectively. Despite its simplicity, the model reproduces first order characteristics observed at Soultz-sous-Forêts, in particular the phenomenon of the largest magnitude events occurring several days after shut-in of the injection well.

Understanding the latter phenomenon has been outlined as a key challenge for the EGS technology [1]. Several numerical approaches have been suggested for simulating induced seismicity (see [1] and references therein). Existing numerical models usually associate fluid overpressure with induced seismicity using a Coulomb friction criterion, but without implementing a physical model describing the strength of the seismicity (e.g. [19–22]). Earthquake magnitudes are treated as a statistical parameter by some *a priori* assumptions on fracture– and/or magnitude–frequency distributions (e.g. [23]). This is different in the current study, where simulated earthquake magnitudes are based on a physical model.

5.1. Geometrical model

Previous analysis of the induced seismicity at Soultz-sous-Forêts yields contradicting results concerning the spatial distribution of the induced seismicity. Michelet and Toksöz [24] apply the collapsing method described in Jones and Stewart [12] to seismicity induced during the stimulation of GPK3 and obtain a volumetric rather than a planar distribution. Charlety et al. [25] analyse the hypocenter distribution of the larger magnitude events ($M \geq 1.4$, occurring during the stimulation of GPK2, GPK3, and GPK4) and conclude that the seismicity aligns along large scale (tectonically formed) fractures. The two studies, however, differ in their underlying data base. Michelet and Toksöz [24] use recordings of the local downhole network only (the same data set used in the present study; compare Fig. 2), whereas Charlety et al. [25] additionally incorporate recordings of a local surface station network. By requiring data from at least eight stations for their hypocenter determination, Charlety et al. [25] prevent the scenario of a co-planar network configuration as discussed previously for the ultra-sparse downhole network. Michelet and Toksöz [24] require data from four or more stations for their hypocenter location, independent of the resulting station geometry. During reprocessing of the same data set we find this selection criterion to be insufficient to ensure a well-constrained hypocenter inversion problem. In particular, we notice that hypocenter location confidence estimates—which form the basis for the data collapsing technique applied by Michelet and Toksöz [24]—might dramatically underestimate true location errors whenever the network configuration tends to be co-planar. Therefore, we conclude that a planar hypocenter distribution, as found by Charlety et al. [25] and in the current study, is a better approximation of the actual reservoir geometry. Finer structures may still be identified in the hypocenter distribution (Fig. 3, bottom). In the context of our numerical model we note, however, that the mechanical interaction between different fault branches is difficult to assess and therefore we restrict ourselves to the simplified model of a single fault zone.

5.2. Hydraulic model parameter

Hydraulic parameters have been estimated from various tests conducted in GPK2, GPK3, and GPK4, respectively. Since the reservoir has been subjected to major changes in the course of hydraulic stimulations, parameters for the initial state of the reservoir (i.e. prior to stimulation activities) are best estimated from GPK2 pre-stimulation tests. Hydraulic parameters listed in Table 2 are based on a well test analysis conducted in GPK2 prior to stimulation [17]. These values were slightly adjusted to better fit observed data with simulation results. A high storage coefficient (compare Table 2) was introduced to account for elastic effects of the fracture which are not implemented in the numerical model.

The value for the permeability enhancement was set to 10% enhancement per slip with the total enhancement being limited to 100 times the initial value. Besides matching observed peak pressures at the injection well, a guideline for fine-tuning these values stems from a comparison of pre- to post-stimulation hydraulic tests indicating a 20-fold increase of the injectivity caused by the GPK2 stimulation [4]. Although our numerical models exhibit a 100-fold increase in the vicinity of the injection

well, permeability enhancement further away from the well is not saturated and decreases with distance from the injection well. On average, a 20-fold permeability increase is obtained when accounting for distances of several 100 m from the injection well.

Compared to the observed pressure response during stimulation of GPK2 (Fig. 1, top), peak values of the modelled wellhead pressure exceed observed values by approximately 20 bars (Fig. 5). It should be noted, however, that the numerical model does not account for a hydraulic skin around the injection well which is found to be negative [17] thus reducing simulated overpressures. We also notice that the simulated pressure decay in the post-injection period is more rapid than the pressure decay observed after the GPK2 stimulation. This difference might be caused by the simplifying assumption of the rock matrix being hydraulically impermeable. If the matrix is not entirely impermeable, then the matrix contribution in the post-injection period would decelerate the pressure decay at the wellhead.

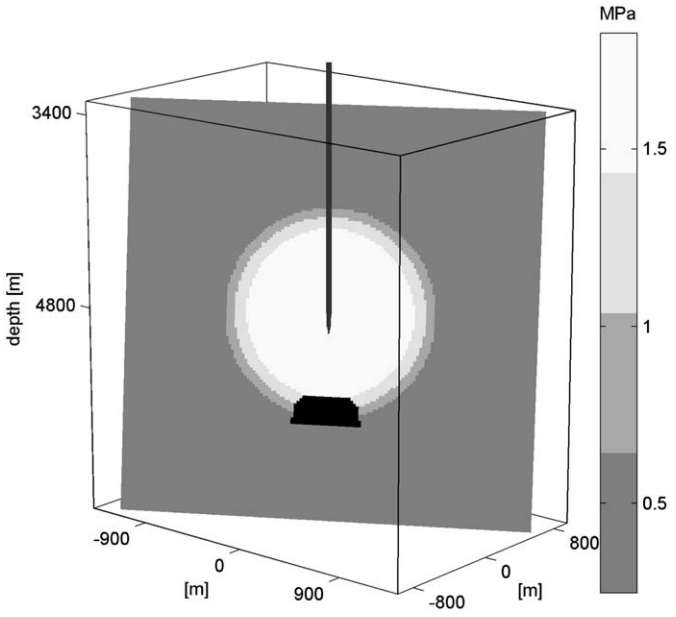

Fig. 8. Distribution of hydraulic overpressures inside the fault zone at the time when the largest magnitude event occurred (12.3 days). Grey shading denotes pressures in MPa according to the grey map. Solid line denotes the location of the injection well. Patches that slipped in the course of the largest magnitude event are marked in black. The largest magnitude event occurred at the outer rim of the previously stimulated region.

5.3. Stress transfer

In our simplified model, the two key parameters controlling mechanical interactions between fault patches are (i) the stress drop and (ii) the stress transfer to neighbouring patches (Fig. 4). With increasing stress drop, the maximum observed magnitude increases while the total number of induced events decreases. When the stress transfer to neighbouring patches is increased, both the size and the total number of events increase. Both observations are physically plausible. High stress drop values trigger larger events as more energy is distributed to neighbouring patches, thus increasing the likelihood for slip avalanches. For the extreme case of using no stress transfer at all, we note that only events with the minimum magnitude occur in our numerical simulations (i.e. one slipped patch per event only).

Event magnitudes, stress drop, and the total number of events are parameters that can be observed in real data and thus can be used for calibrating the stress-transfer parameters. Charlety et al. [25] find indications that the stress drop of the induced seismicity at Soultz-sous-Forêts is in the range between 0.1 and 10 MPa. Given their results we assume a constant stress drop of 1 MPa in our numerical simulations. By approximately matching maximum magnitudes and the total number of events observed during the GPK2 stimulation, we find that the amount of stress transfer to neighbouring patches is on the order of 90%, whereas the shape of the redistribution pattern (Fig. 4) has been assumed *a priori*. Testing different redistribution patterns we find that our modelling results are not critically depending on the shape of the redistribution pattern, as long as the amount of stress transfer remains the same.

5.4. Post-injection seismicity

At first glance, the occurrence of post-injection seismicity seems to contradict the assumed triggering mechanism of Coulomb friction where increasing fluid pressure controls the seismic activity. Simple hydraulic considerations, however, demonstrate that pressure diffusion may lead to a local increase of the hydraulic pressure even in the shut-in period after an injection has been terminated (e.g. [6]). This effect occurs whenever the

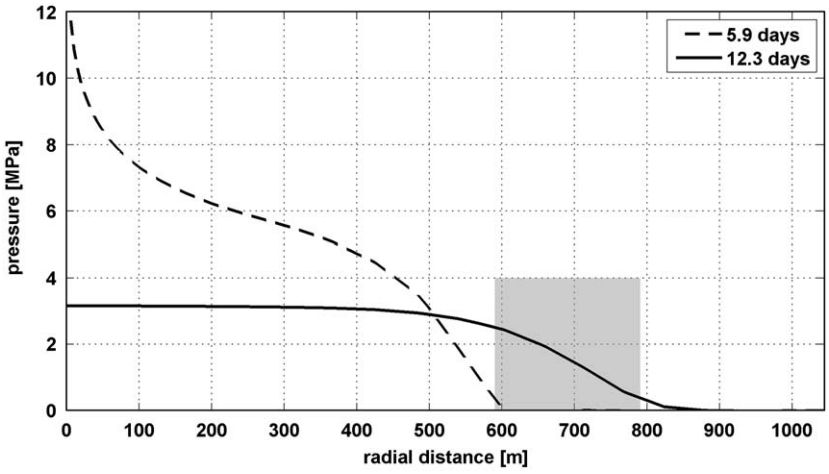

Fig. 9. Hydraulic overpressures inside the fault zone as a function of radial distance to the injection well for the time of shut-in (dashed line) and for the time when the largest magnitude event occurred (solid line). The shaded area marks the location of those patches slipping in the course of the largest magnitude event. At these locations, fluid overpressure increased after shut-in.

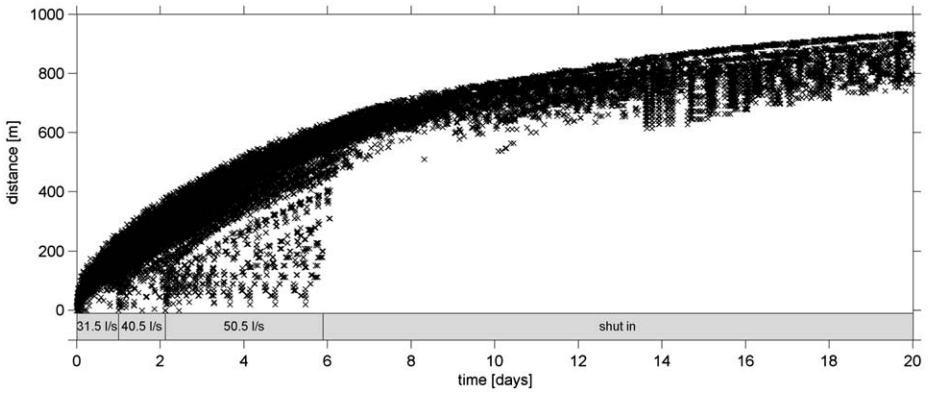

Fig. 10. Radial distance of seismic events to the injection well plotted against time. Bottom bar indicates the injection history.

fluid pressure has not reached stationary conditions during an injection. Fig. 8 shows the spatial distribution of hydraulic overpressures at the time when the largest magnitude event occurred. The location of this event is at the outer rim of the zone of previous seismic activity. Here, fluid overpressures keep increasing after shut-in, exhibiting relatively shallow spatial gradients (Fig. 9). Therefore, many neighbouring patches are on a similar level of stress criticality (Eq. (1)) thus increasing the likelihood for the occurrence of slip avalanches (i.e. large magnitude events), where only a small amount of stress-diffusion is sufficient to cause overcritical conditions over a larger area.

These observations suggest that the maximum event magnitude is predominantly controlled by the area over which fluid pressure elevation brings stress conditions close to criticality. Due to this geometrical effect, the maximum magnitude of events occurring during a stimulation experiment tends to increase with injection time. In parallel, the location of seismic activity systematically migrates away from the injection well when the injection pressure remains constant. This so-called Kaiser effect [26] becomes most evident in Fig. 10 showing radial distance from the injection well as a function of time for the modelled seismicity. The region near the injection well starts getting seismically quiet with increasing time and near-well seismicity occurs predominantly when the injection rate (and thus the injection pressure) is increased. A small number of near-well events occurring through the entire injection period reflect the slow pressure increase which has been observed during the constant rate injection (Fig. 5). At the time of shut-in, near-well seismicity immediately vanishes (Fig. 10) because fluid overpressures in the near-well region start decreasing. Such a clear manifestation of the Kaiser effect is typically observed after massive stimulations of deep geothermal reservoirs, for example at Soultz-sous-Forêts (Fig. 2 in [6]), at Basel (Fig. 7 in [3]), and in the Australian Cooper Basin (Fig. 7 in [11]).

6. Conclusions

We presented a data set of more than 114,000 microearthquakes induced during the stimulation of the deep geothermal reservoir at Soultz-sous-Forêts. Seismicity occurred on a subvertical, approximately two-dimensional structure which might reflect a pre-existing feature of the Rhine–Graben complex.

Based on these findings we developed a numerical, finite-element model to simulate hydraulic overpressures and induced seismicity occurring on a fault structure. The model is based on the physical processes of fluid pressure and stress diffusion with triggering of the induced seismicity being controlled by Coulomb friction. Modelled seismicity exhibits similar characteristics as the seismicity observed during stimulations at Soultz-sous-Forêts. The total number of events and the magnitude–frequency distribution of the modelled seismicity approximately match observations made during the stimulation of the GPK2 well. Consistent with observations at Soultz-sous-Forêts, hypocenters of the modelled seismicity systematically migrate away from the injection well with increasing time (Kaiser Effect). An intriguing observation made at Soultz-sous-Forêts and elsewhere is that the largest magnitude events occur in the post-injection period. Based on modelled seismicity, we demonstrate that these post-injection events can be attributed to a simple geometrical effect without invoking other triggering mechanisms than pressure and stress diffusion.

Recent analysis of the induced seismicity at the geothermal sites at Basel (e.g. [3]) and in the Cooper Basin [11,27] indicates that other geothermal reservoirs might also be dominated by two-dimensional structures. Therefore we feel that the numerical model presented here for Soultz-sous-Forêts can also be applied to other geothermal reservoirs and may provide a powerful tool for addressing the seismic risk associated with reservoir stimulations.

Acknowledgements

A pilot study "Seismic risk associated with the stimulation of geothermal reservoirs: A case study of the deep reservoir at Soultz-sous-Forêts" was carried out by Q-con for LIAG (Leibniz-Institut für Angewandte Geophysik). This pilot study was supported by the Federal Ministry for the Environment, Nature Conservation and Nuclear Safety (BMU), and the European Commission (EC) under Contracts no. 032 99 50 B and SES6-CT-502706, respectively. The views and judgements expressed in the paper are those of the authors and do not necessarily reflect those of BMU or EC. We are especially grateful to the European Economic Interest Grouping (EEIG) "Heat Mining" for cooperation and providing us with seismic data from the hot dry rock project Soultz. Particularly we want to thank Marion Schindler (Federal Institute for Geosciences and Natural Resources, BGR; now BESTEC GmbH) and the scientific coordinator of the Soultz Project Albert Genter. Discussions with many scientists from the European Hot Dry Rock Association (EHDRA) were extremely helpful. Comments by Wolfgang Wirth also helped. Last but not least, the authors would like to thank Julian Bommer and an

anonymous reviewer for their constructive critiques and helpful suggestions.

References

[1] Majer EL, Baria R, Stark M, Oates S, Bommer J, Smith B, et al. Induced seismicity associated with enhanced geothermal systems. Geothermics 2007;36:185–222.
[2] Davis SD, Frohlich C. Did (or will) fluid injection cause earthquakes?—Criteria for a rational assessment. Seismol Res Lett 1993;64(3–4):207–24.
[3] Häring MO, Schanz U, Ladner F, Dyer BC. Characterisation of the Basel 1 enhanced geothermal system. Geothermics 2008;37(5):469–95.
[4] Dorbath L, Cuenot N, Genter A, Frogneux M. Seismic response of the fractured and faulted granite of Soultz-sous-Forêts (France) to 5 km deep massive water injections. Geophys J Int 2009;177(2):653–75.
[5] Bommer JJ, Oates S, Cepeda JM, Lindholm C, Bird J, Torres R, et al. Control of hazard due to seismicity induced by a hot fractured rock geothermal project. Eng Geol 2006;83:287–306.
[6] Baisch S, Weidler R, Vörös R, Jung R. A conceptual model for post-injection seismicity at Soultz-sous-Forêts. Trans Geotherm Resour Counc 2006;30:601–6.
[7] Bear J. Dynamics of fluids in porous media. New York: American Elsevier; 1972.
[8] Bak P, Tang C. Earthquakes as a self-organized critical phenomenon. J Geophys Res 1989;94(B11):15635–7.
[9] Chen Z, Narayan SP, Yang Z, Rahman SS. An experimental investigation of hydraulic behaviour of fractures and joints in granitic rock. Int J Rock Mech Min Sci 2000;37:1061–71.
[10] Baisch S, Bohnhoff M, Ceranna L, Tu Y, Harjes HP. Probing the crust to 9 km depth: Fluid injection experiments and induced seismicity at the KTB superdeep drilling hole, Germany. Bull Seismol Soc Am 2002;92:2369–80.
[11] Baisch S, Weidler R, Vörös R, Wyborn D, DeGraaf L. Induced seismicity during the stimulation of a geothermal HFR reservoir in the Cooper Basin (Australia). Bull Seismol Soc Am 2006;96(6):2242–56.
[12] Jones RH, Stewart RC. A method for determining significant structures in a cloud of earthquakes. J Geophys Res 1997;102(B4):8245–54.
[13] Weidler R, Gerard A, Baria R, Baumgaertner J, Jung R. Hydraulic and microseismic results of a massive stimulation test at 5 km depth at the European hot-dry-rock test site Soultz, France. In: Proceedings of 27th workshop on geothermal reservoir engineering, Stanford University; 2002.
[14] Cornet F, Berard Th, Bourouis S. How close to failure is a granite rock mass at a 5 km depth?. Int J Rock Mech Min Sci 2007;44:47–66.
[15] Healy JH, Hamilton RM, Raleigh CB. Earthquakes induced by fluid injection and explosion. Tectonophysics 1970;9:205–14.
[16] Hainzl S, Zöller G, Kurths J. Self-organization of spatio-temporal earthquake clusters. Nonlinear Processes Geophys 2000;7:21–9.
[17] Tischner T, Pfender M, Teza D. Hot Dry Rock Project Soultz: Erste Phase der Erstellung einer wissenschaftlichen Pilotanlage Final Report, Fed Inst Geosci Nat Resour 2006: 85 pages [in German].
[18] Bungum H, Vaage S, Husebye ES. The Meloy Earthquake Sequence, Northern Norway: Source parameters and their scaling relations. Bull Seismol Soc Am 1982;72(1):197–206.
[19] Shapiro SA, Huenges E, Borm G. Estimating the crust permeability from fluid-injection-induced seismic emission at the KTB site. Geophys J Int 1997;131:F15–8 [see also Corrigendum, Geophys J Int 1998;134:913].
[20] Rothert E, Shapiro SA. Microseismic monitoring of borehole fluid injections: data modeling and inversion for hydraulic properties of rocks. Geophysics 2003;68(2):685–9.
[21] Parotidis M, Shapiro SA, Rothert E. Back front of seismicity induced after termination of borehole fluid injection. Geophys Res Lett 2004;31:L02612, doi:10.1029/2003GL018987.
[22] Kohl T, Mégel T. Coupled hydro-mechanical modelling of the GPK3 reservoir stimulation at the European EGS site Soultz-sous-Forêts. In: Proceedings of the 13th workshop on geothermal reservoir engineering, Stanford University; 2005, SGP-TR-176.
[23] Shapiro SA, Dinske C, Kummerow J. Probability of a given-magnitude earthquake induced by a fluid injection. Geophys Res Lett 2007;34:L22314, doi:10.1029/2007GL031615.
[24] Michelet S, Toksöz MN. Fracture mapping in the Soultz-sous-Forêts geothermal field using microearthquake locations. J Geophys Res 2007;112:B07315, doi:10.1029/2006JB004442.
[25] Charlety J, Cuenot N, Dorbath L, Dorbath C, Haessler H, Frogneux M. Large earthquakes during hydraulic stimulations at the geothermal site of Soultz-sous-Forêts. Int J Rock Mech Min Sci 2007;44(8):1091–105.
[26] Baisch S, Harjes HP. A model for fluid injection induced seismicity at the KTB. Geophys J Int 2003;152:160–70.
[27] Baisch S, Vörös R, Weidler R, Wyborn D. Investigation of fault mechanisms during geothermal reservoir stimulation experiments in the Cooper Basin (Australia). Bull Seismol Soc Am 2009;99(1):148–58.
[28] Brüstle W, Stange S. Ann Bull State Surv Geol Nat Resour Min, Baden-Wuerttemberg, 2000. 〈http://www.lgrb.uni-freiburg.de/lgrb/Fachbereiche/erdbebendienst/jahresbulletins〉.